Lattice vibrations in single-wall carbon nanotubes

D. Gunlycke, H. M. Lawler,* and C. T. White
Naval Research Laboratory, Washington, DC 20375, USA
(Received 16 October 2007; published 30 January 2008)

We present a study of lattice vibrations in single-wall carbon nanotubes. The study is based on a force-constant model, where the force constants are obtained from a general invariant potential that includes up to fourth-nearest-neighbor interactions. Applying the model, we obtain phonon dispersions and density of states for various types of nanotubes. General low-frequency modes such as ring modes and longitudinal modes are also identified and investigated. They are almost independent of the chiral angle but significantly dependent on the radius. The radius dependence is used for scaling, leading to a universal density of states at low frequencies.

DOI: 10.1103/PhysRevB.77.014303 PACS number(s): 63.20.D−, 63.22.−m, 81.07.De

I. INTRODUCTION

Fundamental to the description of many physics properties in a solid are the energy dispersion and density of states. In particular, the phonon energy dispersion and density of states are useful in describing lattice vibrations and mechanical and thermal transport. Because phonons couple to other excitations or particles, they are also needed to understand more advanced phenomena such as electron-phonon scattering and superconductivity.

There are several methods available for obtaining phonon energy dispersions in single-wall carbon nanotubes, ranging from the use of first-principles codes to analytical derivations in the continuum limit. One common approach is to apply a classical or continuum model.[1–8] These models describe long-wavelength phonons well and can concomitantly produce good dispersions in the low- and high-energy regimes. However, if one is interested in the entire phonon dispersions, including the large intermediate energy regime, one has to explicitly consider the atomic structure. Many phonon calculations have been based on translational symmetry along the nanotube axis and have been performed using force-constant,[3,9–14] tight-binding,[15–17] and first-principles models.[18–25] While translational symmetry might be intuitive, it does not encompass the full symmetry of a nanotube; consequently, large unit cells must be used, particularly for chiral nanotubes. The numerical demand caused by the large unit cells sometimes rules out a significant subset of nanotubes for consideration. The alternative is to adopt helical and rotational symmetries,[26] which shrinks the number of atoms in unit cells or helical motifs in nanotubes down to 2. These symmetries are increasingly being employed in force-constant[27–32] and tight-binding[33–38] calculations. First-principles calculations of phonon dispersions based on helical and rotational symmetries have yet to be performed.

In the next section, we describe a force-constant model, similar to that of Gartstein,[31] which includes up to fourth-nearest-neighbor interactions. The model is of valence-force-field type with force constants obtained from an invariant potential that is constructed from internal coordinates. The force constants obtained from this potential automatically obey sum rules associated with rigid translations of a nanotube and rotations about its axis. The sum rules are expressed in a compact form using cylindrical coordinates. We also express analytical derivatives of the internal coordinates and describe how we obtain the coefficients in the invariant potential. Combined with helical and rotational symmetries, we can generate energy dispersions and density of states for all types of nanotubes in a systematic fashion.

Numerical results from our model are presented and discussed in Sec. III. Low-frequency phonon modes are characterized, and their behavior is compared to predictions from continuum theory. Nanotubes with different radii and chiral angles are also compared, leading to the observation of a universal scaling behavior at low frequencies of the first few van Hove peaks in the density of states, a scaling behavior that follows from the cylindrical geometry of the nanotubes. A universal scaling behavior has also been observed in the electronic density of states,[39] but that behavior has a different origin. Some concluding remarks are then made in Sec. IV.

II. THEORY

A. Nanotube structure

The structure of all single-wall carbon nanotubes can be viewed as strips of graphene rolled up to the shape of a cylinder. Different nanotubes are distinguished by the size of the strips and their orientation relative to the underlying honeycomb lattice. These two degrees of freedom can be related to a set of numbers (n_1,n_2), which are defined by the roll-up vector

$$\vec{R} = n_1\vec{R}_1 + n_2\vec{R}_2, \tag{1}$$

where $\vec{R}_1 \equiv a\hat{x}$ and $\vec{R}_2 \equiv (a/2)\hat{x} + (a\sqrt{3}/2)\hat{y}$ are primitive lattice vectors of graphene with $a \approx 0.246$ nm. The roll-up procedure is made in such a way that two points directly across on the graphene strip separated by the roll-up vector are mapped onto the same point on a nanotube. This mapping defines the radius and chiral angle of that particular nanotube,

$$r = \frac{a}{2\pi}\sqrt{n_1^2 + n_1n_2 + n_2^2},$$

$$\Theta = \arctan\left(\frac{\sqrt{3}n_2}{2n_1+n_2}\right). \tag{2}$$

Coordinates on a nanotube can easily be described using a cylindrical coordinate system (ρ,ϕ,z), with the fixed radius $\rho=r$. Given an arbitrary location of an atom ξ_A on a cylindrical shell with radius r, a neighboring atom can be found at $\xi_B=\hat{\mathcal{R}}_z(\phi_0')\hat{\mathcal{T}}_z(h_0')\xi_A$, where $\hat{\mathcal{R}}_z$ and $\hat{\mathcal{T}}_z$ are the rotation and translation operators about and along the nanotube axis, and

$$\phi_0' = \frac{(n_1+n_2)\pi}{n_1^2+n_1n_2+n_2^2},$$

$$h_0' = \frac{(n_1-n_2)a}{2\sqrt{3}\sqrt{n_1^2+n_1n_2+n_2^2}}. \tag{3}$$

Using these two atoms as a basis, we can now map the remaining atoms in the crystal by applying the rotational and helical symmetry operators[26,40] $\hat{\mathcal{C}}_N \equiv \hat{\mathcal{R}}_z(2\pi/N)$ and $\hat{\mathcal{S}} \equiv \hat{\mathcal{R}}_z(\phi_0)\hat{\mathcal{T}}_z(h_0)$, respectively. N is the greatest common divisor of n_1 and n_2, and ϕ_0 and h_0 can be taken as

$$\phi_0 = \frac{[(2p_1+p_2)n_1+(2p_2+p_1)n_2]\pi}{n_1^2+n_1n_2+n_2^2},$$

$$h_0 = \frac{\sqrt{3}Na}{2\sqrt{n_1^2+n_1n_2+n_2^2}}, \tag{4}$$

where p_1 and p_2 are integers that must satisfy the linear Diophantine equation $p_2n_1-p_1n_2=\pm N$ to ensure that each helical motif contains exactly two atoms. The unperturbed atomic coordinates in the nanotube can now be expressed as

$$x_{lm\tau}^{(0)} = \hat{\mathcal{C}}_N^l \hat{\mathcal{S}}^m \xi_\tau, \tag{5}$$

where $0 \leqslant l < N$, m ranges over all integers, and $\tau \in \{A,B\}$ denotes the basis atom.

The eigenvalue equations of the symmetry operators $\hat{\mathcal{C}}_N$ and $\hat{\mathcal{S}}$ are

$$\hat{\mathcal{C}}_N|n\rangle = e^{2\pi i n/N}|n\rangle, \quad n=0,\ldots,N-1,$$

$$\hat{\mathcal{S}}|\kappa\rangle = e^{i\kappa}|\kappa\rangle, \quad -\pi \leqslant \kappa < \pi, \tag{6}$$

with the eigenvectors $|n\rangle$ and $|\kappa\rangle$ given by

$$|n\rangle = \frac{1}{\sqrt{N}}\sum_{l=0}^{N-1} e^{-2\pi i n l/N}|l\rangle,$$

$$|\kappa\rangle = \lim_{M\to\infty}\frac{1}{\sqrt{2M}}\sum_{m=-M}^{M-1} e^{-i\kappa m}|m\rangle. \tag{7}$$

It is also useful to form combined states,[26,40] $|n,\kappa\rangle$, where

$$|n,\kappa\rangle = \lim_{M\to\infty}\frac{1}{\sqrt{2NM}}\sum_{l,m} e^{-2\pi i n l/N}e^{-i\kappa m}|l,m\rangle. \tag{8}$$

As we shall see, these combined states block diagonalize the full force-constant matrix, making phonon dispersions and density of states in large-diameter chiral nanotubes tractable.

B. Lattice dynamics

A displacement of any atom in any direction in the nanotube will introduce forces. Defining the displacement of atom $lm\tau$ along the cylindrical coordinate μ as $d_{lm\tau}^\mu \equiv x_{lm\tau}^\mu - x_{lm\tau}^{\mu(0)}$, one can construct the equations of motion

$$M_c h^\mu \ddot{d}_{lm\tau}^\mu = -\frac{1}{h^\mu}\frac{\partial U}{\partial d_{lm\tau}^\mu}, \tag{9}$$

where M_c is the atomic mass of carbon, $h=(1,\rho,1)$ is a cylindrical scaling factor, and U is the potential experienced by the atom. Within the harmonic approximation, the potential can be expressed as

$$U = \frac{1}{2}\sum_{ll'mm'}\sum_{\tau\tau'\mu\nu} h^\mu d_{lm\tau}^\mu \Phi_{\mu\nu}^{\tau\tau'}(l,l',m,m') h^\nu d_{l'm'\tau'}^\nu, \tag{10}$$

where $\Phi_{\mu\nu}^{\tau\tau'}(l,l',m,m')$ are interatomic force constants. In a cylindrical coordinate system, the force constants only depend on l, l', m, and m' through the differences $l-l'$ and $m-m'$, giving

$$\Phi_{\mu\nu}^{\tau\tau'}(l,l',m,m') = \Phi_{\mu\nu}^{\tau\tau'}(l-l',m-m'). \tag{11}$$

This reduction is only possible in a local coordinate system.[31] Because the equations of motion have the symmetry of the lattice, we can use Eq. (8) to write a solution to Eqs. (9) and (10) of the form

$$d_{lm\tau}^\mu(t) = \frac{1}{\sqrt{2NM}} e^{-2\pi i l n/N} e^{-im\kappa} e^{-i\omega t}\epsilon_\tau^\mu, \tag{12}$$

where ω is a phonon frequency and ϵ_τ^μ is a polarization vector. As the force-constant matrix is block diagonal in the $|n,\kappa\rangle$ representation, (n,κ) can be treated as parameters referring to a specific block matrix. The 6×6 block matrix is called the dynamical matrix D, and its elements are given by

$$D_{\mu\nu}^{\tau\tau'}(n,\kappa) \equiv \sum_{l,m} e^{2\pi i l n/N} e^{im\kappa}\Phi_{\mu\nu}^{\tau\tau'}(l,m). \tag{13}$$

Using Eqs. (10)–(13), we can express the equations of motion [Eq. (9)] as an infinite set of independent eigenvalue equations

$$M_c\omega_\eta^2 h^\mu \epsilon_{\tau,\eta}^\mu = \sum_{\tau',\nu} D_{\mu\nu}^{\tau\tau'} h^\nu \epsilon_{\tau',\eta}^\nu, \tag{14}$$

each with six solutions η. A phonon dispersion can now be built up with branches identified by n and η and with κ as the continuous variable. We will return to the practical implementation in a later subsection.

C. Cylindrical sum rules

In the theory of lattice dynamics, the dynamical matrix is known to adhere to sum rules in the long-wavelength limit. These sum rules originate from infinitesimal translational or rotational displacements of the entire structure. As these dis-

placements leave the relative coordinates unchanged, they correspond to zero-frequency vibrations. In nanocrystalline nanowires,[41] including carbon nanotubes,[4,5] there are four zero-frequency modes. In addition to one longitudinal and two transverse modes, corresponding to translations along and perpendicular to the nanotube axis, there is one torsional mode relating to infinitesimal rotations about the same axis. Each type of zero-frequency mode, longitudinal, transverse, and torsional, leads to one sum rule.

The sum rules are obtained by expressing the force on an arbitrary atom and setting that force equal to zero for the appropriate displacements. The force on an atom 00τ, along the cylindrical coordinate μ, can be deduced from the right-hand side of Eq. (9). Using Eqs. (10) and (11), the force takes the form

$$F_{\mu}^{00\tau} = \sum_{l'm'\tau'\nu} \Phi_{\mu\nu}^{\tau\tau'}(-l',-m')h^{\nu}d_{l'm'\tau'}^{\nu}. \tag{15}$$

Turning to the longitudinal sum rule, we know that this force must remain zero if an entire nanotube, which is otherwise in equilibrium, is translated down its axis by an amount of δ^z. As every atom is displaced the same amount, the atomic displacements are simply $d_{l'm'\tau'}^{\rho}=d_{l'm'\tau'}^{\phi}=0$ and $d_{l'm'\tau'}^{z}=\delta^z$. Substituting these displacements into Eq. (15) allows the longitudinal sum rule to be expressed as

$$\sum_{lm\tau'} \Phi_{\mu z}^{\tau\tau'}(l,m) = 0. \tag{16}$$

The torsional sum rule is similarly derived. If a nanotube undertakes an azimuthal rotation of magnitude δ^{ϕ}, no forces will arise. Thus, the torsional sum rule can be expressed as

$$\sum_{lm\tau'} \Phi_{\mu\phi}^{\tau\tau'}(l,m) = 0. \tag{17}$$

Now, consider a transverse translation in, say, the x direction with an amount of δ^x. The displacements can in this case be written as $d_{l'm'\tau'}^{\rho}=\delta^x \cos\phi_{l'm'\tau'}$, $h^{\phi}d_{l'm'\tau'}^{\phi}=-\delta^x \sin\phi_{l'm'\tau'}$, and $d_{l'm'\tau'}^{z}=0$, giving the transverse sum rule

$$\sum_{lm\tau'} [\Phi_{\mu\rho}^{\tau\tau'}(l,m)\cos\phi_{lm\tau'} + \Phi_{\mu\phi}^{\tau\tau'}(l,m)\sin\phi_{lm\tau'}] = 0, \tag{18}$$

where $\phi_{lm\tau'}=2\pi l/N+m\phi_0+\phi_{\tau'}$ with $\phi_A-\phi_B=\phi_0'$ from Eqs. (3)–(5). A translation in any other transverse direction would lead to the same equation but with an additional unimportant phase that could be incorporated in $\phi_{\tau'}$.

In addition to the three sum rules expressed above, there is a fourth exact sum for $n=0$ in the limit $\kappa\to 0$. To understand the origin of this sum rule, we transform the dynamical matrix using parallel (+) and antiparallel (−) polarizations of the A and B sublattices. The new basis elements can be denoted as $\rho+$, $\rho-$, $\phi+$, $\phi-$, $z+$, and $z-$. Now, consider a twofold rotation about an axis that intersects the nanotube axis orthogonally and a point at the center of an arbitrary $A-B$ bond. Such a rotation sends all $\tau=A$ atoms into $\tau=B$ atoms, and vice versa. In addition to exchanging the sublattices, the rotation also changes the sign of the ϕ and z directions. We can therefore conclude that the configurations $\rho+$, $\phi-$, and $z-$ have eigenvalues of 1 under the rotation, while the configurations $\rho-$, $\phi+$, and $z+$ have eigenvalues of -1. This is a very useful observation because there cannot exist any nonzero dynamical matrix elements between two states of opposite symmetries. This is recognized through the fact that the potential energy must be invariant with respect to the application of the twofold rotation. We also know from Eqs. (16) and (17), which can simply be expressed as $\Sigma_{\tau'}D_{\mu\phi}^{\tau\tau'}(0,0)=\Sigma_{\tau'}D_{\mu z}^{\tau\tau'}(0,0)=0$, that the dynamical matrix at $(n,\kappa)=(0,0)$ has zero rows and columns for $\phi+$ and $z+$. Moreover, $\rho-$ must be an eigenstate of the dynamical matrix with eigenvalue $M_c\omega_{\rho-}^2$. Applying this solution to Eq. (14) with the dynamical matrix given by Eq. (13) gives the final sum rule as

$$\sum_{lm} [\Phi_{\rho\rho}^{AA}(l,m) - \Phi_{\rho\rho}^{AB}(l,m)] = M_c\omega_{\rho-}^2. \tag{19}$$

D. Construction of invariant potential using internal coordinates

In the early days of carbon nanotube theory, based on first-principles results,[42] it became apparent that the electronic energy dispersion of the nanotubes could be obtained from the two-dimensional graphene energy dispersion by quantizing the direction orthogonal to the nanotube axis.[42–44] The graphene sheet model for single-wall carbon nanotubes, which has recently been reviewed,[40] has been proven to be a good approximation in the electronic case, despite its lack of curvature effects. The graphene sheet model was also applied to phonons.[9] Unfortunately, this approach, also known as zone folding, has been proven insufficient. To satisfy the sum rules and to obtain the radial breathing mode, one needs to go beyond the graphene sheet model and make calculations based on the true atomic coordinates of a nanotube. One drawback with the latter approach is that there are no readily available force constants for arbitrary nanotubes. In more recent papers,[27,28,31] this problem has been circumvented by generating invariant valence-force-field-type potentials built from internal coordinates. By applying the true nanotube coordinates to these potentials, one could obtain force constants that automatically obey the sum rules in Eqs. (16)–(19). In this paper, we also apply such a potential of the type suggested by Gartstein.[31] The potential, which only depends on variations of bond lengths, bond angles, and dihedral angles between planes formed by three neighboring carbon atoms, could be written in the form

$$U = \sum_{\Omega_1} U_1 + \sum_{\Omega_2} U_2 + \sum_{\Omega_3} U_3 + \sum_{\Omega_4} U_4, \tag{20}$$

where Ω_m, with $m=1,2,3,4$, are the sets of configurations including up to m^{th}-nearest-neighbor interactions. Owing to a large redundancy, the sets only need to contain configurations of the types shown in Fig. 1, including their rotated and mirrored versions. The potential contributions can be expressed as

$$U_1 = \frac{1}{2}C_1\Delta l_{\alpha\beta}^2,$$

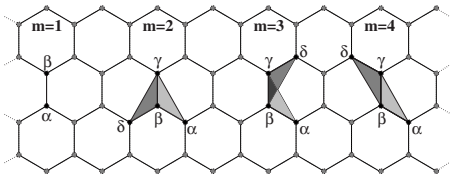

FIG. 1. Configurations containing up to mth-nearest-neighbor interactions.

$$U_2 = C_2\Delta l_{\alpha\beta}\Delta l_{\beta\gamma} + C_3(\Delta l_{\alpha\beta} + \Delta l_{\beta\gamma})\Delta\psi_{\alpha\beta\gamma} + \frac{1}{2}C_4\Delta\psi_{\alpha\beta\gamma}^2 + \frac{1}{2}C_5\Delta\chi_{\alpha\beta\gamma\delta}^2,$$

$$U_3 = C_6\Delta l_{\alpha\beta}\Delta l_{\gamma\delta} + C_7(\Delta l_{\alpha\beta}\Delta\psi_{\beta\gamma\delta} + \Delta l_{\gamma\delta}\Delta\psi_{\alpha\beta\gamma}) + C_8\Delta\psi_{\alpha\beta\gamma}\Delta\psi_{\beta\gamma\delta} + \frac{1}{2}C_9\Delta\chi_{\alpha\beta\gamma\delta}^2,$$

$$U_4 = C_{10}\Delta l_{\alpha\beta}\Delta l_{\gamma\delta} + C_{11}(\Delta l_{\alpha\beta}\Delta\psi_{\beta\gamma\delta} + \Delta l_{\beta\gamma}\Delta\psi_{\alpha\beta\gamma}), \quad C_{12}\Delta\psi_{\alpha\beta\gamma}\Delta\psi_{\beta\gamma\delta} + \frac{1}{2}C_{13}\Delta\chi_{\alpha\beta\gamma\delta}^2, \tag{21}$$

where Δl, $\Delta\psi$, and $\Delta\chi$ are changes in bond length, bond angle, and dihedral angle, respectively. The variations of these internal coordinates, $S=\Delta l$, $\Delta\psi$, $\Delta\chi$, with respect to the Cartesian displacement vectors of the involved atoms, $\vec{u}_t$, can—to first order—be expressed as[45]

$$S = \sum_{t=1}^{n} \vec{s}_t \cdot \vec{u}_t, \tag{22}$$

where n is the number of involved atoms and $\vec{s}_t$ are constant vectors given by the geometry of the structure. If the internal coordinate is $S=\Delta l_{\alpha\beta}$, then

$$\vec{s}_\alpha = -\vec{e}_{\alpha\beta}, \quad \vec{s}_\beta = \vec{e}_{\alpha\beta}, \tag{23}$$

where $\vec{e}_{\alpha\beta}$ is the equilibrium unit vector from atom α to atom β. When the internal coordinate is the bond angle between atoms α, β, and γ, where the angle is formed at atom β, i.e., $S=\Delta\psi_{\alpha\beta\gamma}$, we have

$$\vec{s}_\alpha = \frac{\vec{e}_{\beta\alpha}\cos\psi_{\alpha\beta\gamma} - \vec{e}_{\beta\gamma}}{l_{\beta\alpha}\sin\psi_{\alpha\beta\gamma}},$$

$$\vec{s}_\beta = \frac{\vec{e}_{\beta\alpha}(l_{\beta\alpha} - l_{\beta\gamma}\cos\psi_{\alpha\beta\gamma})}{l_{\beta\alpha}l_{\beta\gamma}\sin\psi_{\alpha\beta\gamma}} + \frac{\vec{e}_{\beta\gamma}(l_{\beta\gamma} - l_{\beta\alpha}\cos\psi_{\alpha\beta\gamma})}{l_{\beta\alpha}l_{\beta\gamma}\sin\psi_{\alpha\beta\gamma}},$$

$$\vec{s}_\gamma = \frac{\vec{e}_{\beta\gamma}\cos\psi_{\alpha\beta\gamma} - \vec{e}_{\beta\alpha}}{l_{\beta\gamma}\sin\psi_{\alpha\beta\gamma}}, \tag{24}$$

where $l_{\alpha\beta}$ is an equilibrium bond length between atoms α and β, and $\psi_{\alpha\beta\gamma}$ is the equilibrium bond angle. The last internal coordinate $S_k=\Delta\chi_{\alpha\beta\gamma\delta}$ is the dihedral angle between the planes spanned by atoms α, β, and γ and atoms β, γ, and δ, and it has

$$\vec{s}_\alpha = \frac{\vec{e}_{\beta\alpha}\times\vec{e}_{\beta\gamma}}{l_{\beta\alpha}\sin^2\psi_{\alpha\beta\gamma}},$$

$$\vec{s}_\beta = \frac{\vec{e}_{\beta\alpha}\times\vec{e}_{\beta\gamma}(l_{\beta\alpha}\cos\psi_{\alpha\beta\gamma} - l_{\beta\gamma})}{l_{\beta\alpha}l_{\beta\gamma}\sin^2\psi_{\alpha\beta\gamma}} - \frac{\vec{e}_{\gamma\delta}\times\vec{e}_{\gamma\beta}\cos\psi_{\beta\gamma\delta}}{l_{\beta\gamma}\sin^2\psi_{\beta\gamma\delta}},$$

$$\vec{s}_\gamma = \frac{\vec{e}_{\gamma\delta}\times\vec{e}_{\gamma\beta}(l_{\gamma\delta}\cos\psi_{\beta\gamma\delta} - l_{\gamma\beta})}{l_{\gamma\delta}l_{\gamma\beta}\sin^2\psi_{\beta\gamma\delta}} - \frac{\vec{e}_{\beta\alpha}\times\vec{e}_{\beta\gamma}\cos\psi_{\alpha\beta\gamma}}{l_{\gamma\beta}\sin^2\psi_{\alpha\beta\gamma}},$$

$$\vec{s}_\delta = \frac{\vec{e}_{\gamma\delta}\times\vec{e}_{\gamma\beta}}{l_{\gamma\delta}\sin^2\psi_{\beta\gamma\delta}}. \tag{25}$$

Previously, we expressed a relationship between the potential energy and force constants [see Eq. (10)]. To obtain the force constants for a given potential, one uses a reversed expression,

$$\Phi_{\mu\nu}^{\tau\tau'}(l-l',m-m') = \frac{1}{h^\mu h^\nu}\frac{\partial^2 U}{\partial d_{lm\tau}^\mu \partial d_{l'm'\tau'}^\nu}. \tag{26}$$

The derivatives in Eq. (26) pass through Eqs. (20) and (21) to the internal coordinates in Eq. (22), and we get terms with factors of the form

$$\frac{1}{h^\mu}\frac{\partial S}{\partial d_{lm\tau}^\mu} = \sum_{t=1}^{n} \vec{s}_t \cdot \frac{1}{h^\mu}\frac{\partial \vec{u}_t}{\partial d_{lm\tau}^\mu}. \tag{27}$$

As the derivatives are zero unless atom t and $lm\tau$ are the same, in which case they are

$$\frac{\partial \vec{u}_t}{\partial d_{lm\tau}^\rho} = (\cos\phi_{lm\tau}, \sin\phi_{lm\tau}, 0)^T,$$

$$\frac{1}{h^\phi}\frac{\partial \vec{u}_t}{\partial d_{lm\tau}^\phi} = (-\sin\phi_{lm\tau}, \cos\phi_{lm\tau}, 0)^T,$$

$$\frac{\partial \vec{u}_t}{\partial d_{lm\tau}^z} = (0,0,1)^T, \tag{28}$$

the sum in Eq. (27) contains at most one term.

The coefficients in Eq. (21) can be determined from force constants in graphene.[9,46,47] In a nearest-neighbor model ($U_2=U_3=U_4=0$), the parameter C_1 is proportional to the in-plane radial force constant $\phi_r^{(1)}$. Including U_2 gives a second-nearest-neighbor model, where $(C_i)_{i=1}^5$ are uniquely determined by the in-plane constants $\phi_r^{(1)}$, $\phi_{ti}^{(1)}$, $\phi_r^{(2)}$, and $\phi_{rt}^{(2)}$ and the out-of-plane constant $\phi_{to}^{(1)}$. The nearest-neighbor in-plane mixing term $\phi_{rt}^{(1)}$ must be zero by symmetry. The remaining two constants, $\phi_{ti}^{(2)}$ and $\phi_{to}^{(2)}$, follow from rotational invariance, which in this case is $\phi_t^{(1)}+6\phi_t^{(2)}=0$. U_3 introduces four more coefficents $(C_i)_{i=6}^9$, but there are only three new third-nearest-neighbor force constants because of symmetry [$\phi_{rt}^{(3)}=0$]. The redundancy is eliminated by enforcing the rotational invariance of the in-plane tangential force constants.

TABLE I. Coefficients derived from graphene force constants presented by Jishi *et al.* (Ref. 9) Grüneis *et al.* (Ref. 46), and Samsonidze *et al.* (Ref. 47). $\phi_{rt}^{(2)}$ and $\phi_{rt}^{(4)}$ are assumed to be zero, and $\phi_{ti}^{(4)}$ and $\phi_{to}^{(4)}$ have been recalculated to obey rotational invariance.

Coefficient	Jishi *et al.* (Ref. 9)	Grüneis *et al.* (Ref. 46)	Samsonidze *et al.* (Ref. 47)
C_1	6.0877	5.4253	5.6173
C_2	1.1254	1.1115	0.8063
C_3	5.6785	3.4892	3.8804
C_4	0.7013	−1.8095	−3.0015
C_5	0.1557	0.1800	0.1779
C_6	2.3437	3.3775	3.9337
C_7	0.5938	0.3808	0.1004
C_8	−0.2813	−1.1175	−1.8163
C_9	0.0281	−0.0112	−0.0112
C_{10}	−1.5928	1.1502	3.3811
C_{11}	0.2690	−0.0072	0.1032
C_{12}	−0.5454	0.2663	0.6981
C_{13}	0.2148	0.2325	0.2293

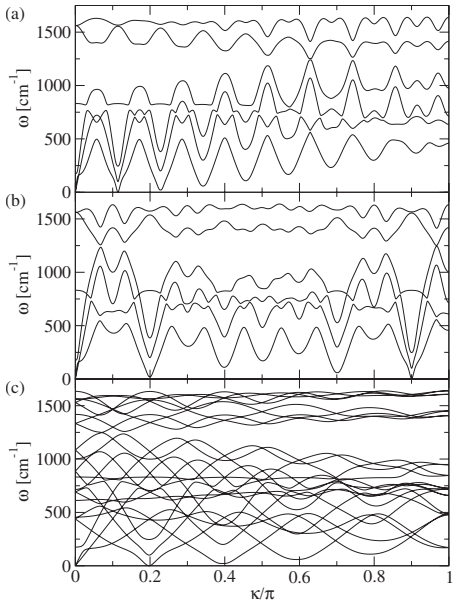

FIG. 2. Phonon dispersions of single-wall carbon nanotubes. The nanotubes in (a)–(c) are (17,1), (11,9), and (12,8), respectively.

The one-to-one mapping is also present in the fourth-nearest-neighbor model where the 13 parameters in the potential are determined by 12 free force constants and 1 force constant with the rotational constraint $\phi_{ti}^{(1)}+6\phi_{ti}^{(2)}+4\phi_{ti}^{(3)}+14\phi_{ti}^{(4)}=0$. In addition to these 13 force constants, there are also three implicit constants, $\phi_{rt}^{(1)}$, $\phi_{rt}^{(3)}$, and $\phi_{to}^{(4)}$, leading to a total of 16 force constants. The coefficients of the invariant potential in the fourth-nearest-neighbor model can be found in Table I.

To obtain the coefficients, we applied the invariant potential, [Eq. (20)] to the graphene lattice structure. In graphene, one can use Cartesian coordinates, in which case the derivatives simplify to

$$\frac{\partial S}{\partial d_{lm\tau}^{\mu}} = s_{lm\tau}^{\mu}. \tag{29}$$

This equation can also be obtained from Eqs. (27) and (28) in the large-diameter nanotube limit. The coefficients are related to the force constants through a linear system of equations which can be solved numerically. In the numerical calculations presented in this paper, we have used coefficients obtained from the graphene force constants given by Samsonidze *et al.*,[47] slightly modified to satisfy rotational invariance.

III. RESULTS

A. Energy dispersion and phonon modes

The new force constants derived from the invariant potential presented in the last section obey the symmetry requirements of arbitrary nanotubes. As such, they generate dynamical matrices that are consistent with the sum rules. Three of these sum rules [Eqs. (16)–(18) followed from invariance with respect to certain rotations and translations. Corresponding to these movements are four phonon modes that must all have a zero frequency. The locations of the zero-frequency modes can be observed in the phonon energy dispersions shown in Fig. 2. Independent of the roll-up vector, there are two acoustic zero-frequency modes in the $n=0$ branches at $\kappa=0$, describing rigid translational motion along and about the nanotube axis. In addition to these modes, there are two zero-frequency modes corresponding to transverse translations of the nanotube. These modes appear at $\kappa=\pm\phi_0$, where ϕ_0 is given by Eq. (4) and is $35\pi/307$, $271\pi/301$, and $15\pi/76$ for the (17, 1), (11, 9), and (12, 8) nanotubes with dispersions shown in Fig. 2. When $N=1$, these modes must, of course, also have $n=0$. In contrast, when $N>1$, these modes are found among the $n=1$, $N-1$ branches, which is the case in Fig. 2(c), where $N=4$.

The dispersions also contain other important modes, such as the radial breathing mode, ring modes, and longitudinal modes. The ring modes are vibrational modes with only a minuscule dependence on the axial coordinate. They can thus, to a good approximation, be found in the axial long-wavelength limit. The axial wave vector k is related to κ through

$$\kappa = \lambda\phi_0 + h_0 k, \tag{30}$$

where λ is an integer identifying a certain ring mode. Letting $k\to 0$ gives the phases of the ring modes as $\kappa=\lambda\phi_0$. To locate the ring modes in the phonon dispersions, one might also have to subtract an appropriate number of 2π from the phase κ and make use of the reflection properties at Γ. A ring mode λ is located in the η branch with the lowest frequency at the ring mode phase. In Figs. 2(a) and 2(b), where $N=1$, all ring modes are located in the same lowest frequency branch. When $N>1$, which is the case in Fig. 2(c), the ring modes appear in different branches with different indices n. More precisely, a ring mode λ must belong to a branch with either index $n=\lambda \pmod N$ or $N-n=\lambda \pmod N$, depending

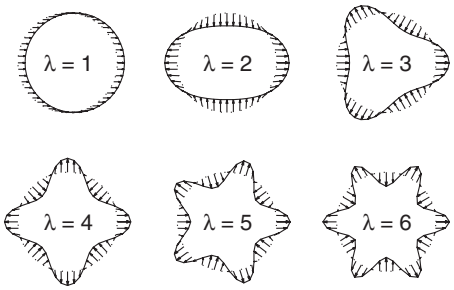

FIG. 3. Ring modes of a (17,1) nanotube. The ring modes obtained using the force-constant approach described in this paper are visually indistinguishable (not shown) from those obtained by Suzuura and Ando using a continuum model (Ref. 5).

on the sign of κ and whether an even or odd number of 2π adjustments was required.

The dynamical matrix exhibits local time-reversal symmetry at the ring mode phases. This symmetry can be seen by substituting Eq. (30) into Eq. (13). As a consequence of this symmetry, first-order perturbation theory predicts that the phonon branches display local extrema at $k=0$. We can see in Fig. 2 that the extrema in the low-energy branches are generally minima. The minima corresponding to $\lambda=1$ represents the zero-frequency mode describing rigid transverse translations. Following the lowest branch in Fig. 2(a) to the right, we see more minima evenly spaced, each representing a ring mode. The vibrational cross sections of these modes are shown in Fig. 3. Virtually identical ring modes can also be found for the nanotubes with dispersions shown in Figs. 2(b) and 2(c).

As the low-energy ring modes are almost independent of the roll-up vector, they can be well described by continuum models. Suzuura and Ando provided an excellent approximation of the ring modes,[5] which can be expressed as

$$\vec{d}_\lambda \approx \lambda \hat{r} \cos \lambda \phi_0 - \hat{\phi} \sin \lambda \phi_0. \tag{31}$$

Using their model, we find that the phonon frequencies corresponding to these ring modes can be approximated as

$$\omega_\lambda \approx \omega_{\mathrm{RM}}^{(0)} \left(\frac{a}{r}\right)^2 (\lambda^2 - 1), \tag{32}$$

where $\omega_{\mathrm{RM}}^{(0)} \approx 54\ \mathrm{cm}^{-1}$ has been obtained using the third parameter set in Table I. This expression is similar to one given by Mahan.[4] As we can see, the ring mode frequencies in Eq. (32) are approximately proportional to the inverse of the square of the radius of the nanotube. This radial dependence is in contrast to that of the radial breathing mode, which has a frequency approximately given by[9]

$$\omega_{\mathrm{RBM}} \approx \omega_{\mathrm{RBM}}^{(0)} \left(\frac{a}{r}\right), \tag{33}$$

where $\omega_{\mathrm{RBM}}^{(0)} \approx 486\ \mathrm{cm}^{-1}$ for the third parameter set in Table I. This estimate of the radial breathing mode frequency coefficient is in good agreement with first-principles calculations,[18,19,48] which give values between 470 and 480 cm^{-1}. The radial breathing mode is found in the $n=0$, η branch with the third lowest or first nonzero frequency at $\kappa=0$. In addition to the ring modes and the radial breathing mode, there can be excited low-energy modes with the same (n,κ) combination as the ring modes but with different η. The lowest such excitation correspond to a mode λ', which is essentially longitudinal. At low frequencies, a longitudinal-mode frequency scales approximately linear with axial wave vector k. For the longitudinal modes, λ in Eq. (30) is strictly zero; thus, $\omega \approx v_l \kappa / h_0$. However, we are interested in special quantized phases, $\kappa = \lambda' \phi_0$. Because ϕ_0/h_0 is inversely proportional to the nanotube radius, we can approximate the frequency of the first excited longitudinal modes as

$$\omega_{\lambda'} \approx \omega_{\mathrm{LM}}^{(0)} \left(\frac{a}{r}\right) \lambda', \tag{34}$$

where $\omega_{\mathrm{LM}}^{(0)} \approx 278\ \mathrm{cm}^{-1}$ for the third parameter set in Table I. This expression is also consistent with Mahan's study of hollow cylinders.[4] The next excitation describes a mode λ'', which again has little axial dependence. Unlike the ring mode, this excited mode has a frequency that scales with the inverse of the radius. With the exception of the two acoustic zero-frequency modes, all modes described in this section where κ is a multiple of ϕ_0 can be identified in the density of states.

B. Density of states

The energy dispersion of a particular nanotube provides excellent information about that nanotube. It is, however, common that one may only require the density of states. The density of states per atom is deduced from the energy dispersion using

$$g(\omega) = \frac{1}{2N} \sum_{n,\eta} \frac{1}{\pi} \int_0^\pi \delta[\omega - \omega_\eta(n,\kappa)] d\kappa. \tag{35}$$

The densities of states of three nanotubes with the same radius but different chiral angles are shown in Fig. 4(a). Their overall structure is similar to that of graphene, but unlike graphene the nanotube density of states exhibits one-dimensional van Hove singularities. These singularities occur at energies where there is an extremum in the energy dispersion. The van Hove singularities can be seen in more detail in Fig. 4(b), which shows a magnification of the low-energy regime. Each singularity has been labeled with a corresponding mode. Because the low-energy modes mostly stem from the cylindrical shape of the nanotubes, the same labels apply to all three nanotubes. Also note that Fig. 4(b) has a singularity at $\omega=0$, which is a consequence of the parabolic energy dependence of the flexure modes in the long-wavelength limit.

The chiral angle has little effect on the density of states at most frequencies [cf. Fig. 4(a)] and, in particular, at the small frequencies displayed in Fig. 4(b). This is not surprising as phonon dispersions are well described at low energy by continuum models that do not explicitly consider the lattice. However, at first inspection, it is not obvious that the six-branch dispersion of a (23,4) or a (17,12) nanotube would

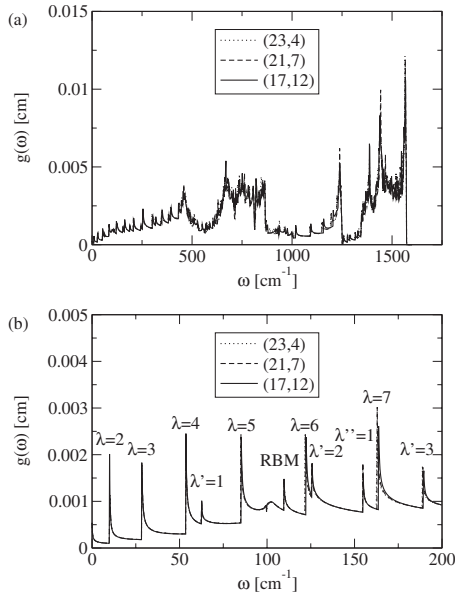

FIG. 4. Density of states per atom of three nanotubes with the same radius but different chiral angles. (a) shows the entire phonon density of states. A low-frequency magnification of the same dispersion is shown in (b). The van Hove singularities in (b) correspond to the radial breathing mode (RBM), ring modes λ, longitudinal modes λ′, and higher-frequency modes λ″.

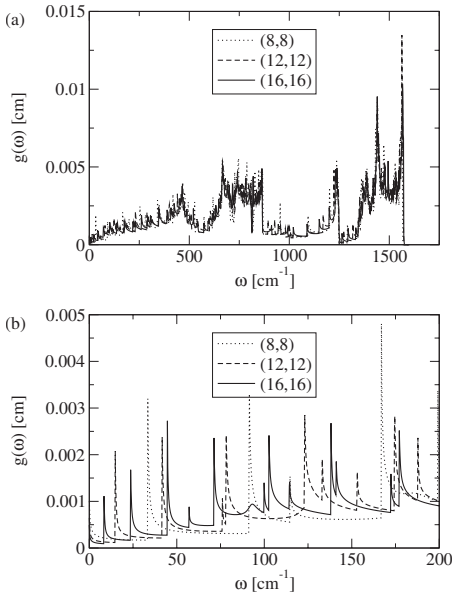

FIG. 5. Density of states per atom of three nanotubes with the same chiral angle. (a) shows the entire phonon density of states and (b) shows a magnification of the low-frequency region.

produce virtually identical densities of states as the 42-branch dispersion of a (21,7) nanotube. On the other hand, the branches in dispersions of nanotubes with smaller N exhibit more oscillations, leading to more van Hove singularities per branch. These oscillations fully compensate for the additional bands in nanotubes with larger N. While the continuum models are accurate at low energy, they might fail at high energy, as lattice effects gradually become more important. Despite that, our force-constant approach shows a remarkable similarity between the densities of states of the three nanotubes even at higher energies. This similarity might be related to the in-plane isotropic nature of the graphene sheet.

To investigate the radial dependence on the density of states for a fixed chiral angle, we have chosen three armchair nanotubes. The density of states of these nanotubes can be seen in Fig. 5. Seen over the entire spectrum, the densities of states of the different nanotubes might appear similar. This similarity comes from the close relationship between the structures of carbon nanotubes and graphene sheets, which share the overall shape of the densities of states. However, at closer inspection, one notices that the densities of states are not as similar as in the case when the radius was fixed [Fig. 4(a)]. The differences are more easily observed in the low-energy regime shown in Fig. 5(b). The van Hove singularities corresponding to the low-energy modes occur at different energies in the different nanotubes, with the exception of the zero-frequency flexure modes.

The peak coincidence at low energies can be recovered by multiplying the energy with dimensionless factors containing the radius or radius squared. In Fig. 6(a), the peaks from the radial breathing modes and the excited modes of different nanotubes overlap. The overlap confirms the approximations in Eqs. (33) and (34). Similarly, the approximation in Eq. (32) can be verified by Fig. 6(b). Note that the densities of states in both figures have been scaled by a dimensionless radius to conserve the atomic density of states in a given

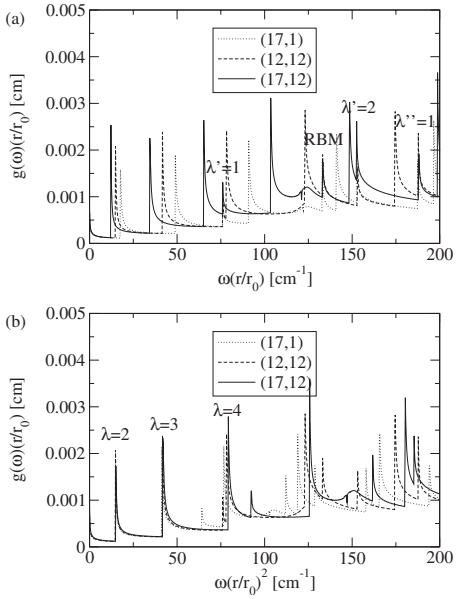

FIG. 6. Scaled density of states per atom. By scaling the density of states and frequency with radius or radius squared, van Hove singularities from arbitrary nanotubes representing a certain mode could be mapped onto each other to a very good approximation. (a) illustrates how peaks from modes with frequencies with inverse radius dependence coincide for three different nanotubes. (b) Low-frequency ring modes can be scaled to produce a low-frequency universal density of states.

mode. The total number of states per atom is independent of the radius. However, the total number of modes is proportional to the radius. Consequently, the first few peaks in Fig. 6(b) are, to a good degree, independent of the roll-up vector. In other words, we have a universal density of states for the first few van Hove peaks. This universal behavior holds for nanotubes with diameters equal to or larger than 1 nm. For nanotubes narrower than 1 nm, the universal behavior eventually breaks down as the ring modes are pushed to higher frequencies.

IV. CONCLUSIONS

Through the use of invariant potentials, we obtained phonon dispersion relations which obey the necessary symmetries required by the structure. Using those relations, we analyzed some modes with high symmetry, particularly ring modes and longitudinal modes, which appear in the low-frequency regime of the density of states. We then used the analyzed modes to label and scale the density of states. This effort could be helpful when trying to identify van Hove singularities in nanotubes where the roll-up vector is unknown. The location of the peaks could also be used to find radii of nanotubes. Attempting to obtain the exact roll-up vector, however, is more challenging, as the studied peaks have little dependence on the chiral angle. Dependence on the chiral angle requires wavelengths of atomic scale. The small chiral-angle dependence was therefore expected in the low-frequency regime where wavelengths are mostly on the scale of nanotube radius. In other words, the search for chiral angle dependence should be more promising in a higher-frequency regime, where lattice effects are more pronounced.

ACKNOWLEDGMENTS

D.G. and H.M.L. thank the Naval Research Laboratory for support through National Research Council Research Associateships. This work was also supported by the Office of Naval Research through the Naval Research Laboratory. C.T.W. thanks P. P. Schmidt for discussions.

*Present address: Department of Physics, University of Washington, Seattle, WA 98195, USA.

[1] D. Kahn, K. W. Kim, and M. A. Stroscio, J. Appl. Phys. **89**, 5107 (2001).
[2] M. A. Stroscio, M. Dutta, D. Kahn, and K. W. Kim, Superlattices Microstruct. **29**, 405 (2001).
[3] S. S. Savinskiĭ and V. A. Petrovskiĭ, Phys. Solid State **44**, 1721 (2002).
[4] G. D. Mahan, Phys. Rev. B **65**, 235402 (2002).
[5] H. Suzuura and T. Ando, Phys. Rev. B **65**, 235412 (2002).
[6] M. Xia, S. Zhang, S. Zhao, and E. Zhang, Physica B **344**, 66 (2004).
[7] S. V. Goupalov, Phys. Rev. B **71**, 085420 (2005).
[8] L. Chico, R. Pérez-Álvarez, and C. Cabrillo, Phys. Rev. B **73**, 075425 (2006).
[9] R. A. Jishi, L. Venkataraman, M. S. Dresselhaus, and G. Dresselhaus, Chem. Phys. Lett. **209**, 77 (1993).
[10] R. Saito, T. Takeya, T. Kimura, G. Dresselhaus, and M. S. Dresselhaus, Phys. Rev. B **57**, 4145 (1998).
[11] A. Charlier, E. McRae, M.-F. Charlier, A. Spire, and S. Forster, Phys. Rev. B **57**, 6689 (1998).
[12] T. Maeda and C. Horie, Physica B **263-264**, 479 (1999).
[13] V. P. Sokhan, D. Nicholson, and N. Quirke, J. Chem. Phys. **113**, 2007 (2000).
[14] G. D. Mahan and G. S. Jeon, Phys. Rev. B **70**, 075405 (2004).
[15] J. Yu, R. K. Kalia, and P. Vashishta, Europhys. Lett. **32**, 43 (1995).
[16] J. Yu, R. K. Kalia, and P. Vashishta, J. Chem. Phys. **103**, 6697 (1995).
[17] M. Menon, E. Richter, and K. R. Subbaswamy, J. Chem. Phys. **104**, 5875 (1996).
[18] J. Kürti, G. Kresse, and H. Kuzmany, Phys. Rev. B **58**, R8869 (1998).
[19] D. Sánchez-Portal, E. Artacho, J. M. Soler, A. Rubio, and P. Ordejón, Phys. Rev. B **59**, 12678 (1999).
[20] O. Dubay and G. Kresse, Phys. Rev. B **67**, 035401 (2003).
[21] L.-H. Ye, B.-G. Liu, D.-S. Wang, and R. Han, Phys. Rev. B **69**, 235409 (2004).
[22] K.-P. Bohnen, R. Heid, H. J. Liu, and C. T. Chan, Phys. Rev. Lett. **93**, 245501 (2004).
[23] D. Connétable, G.-M. Rignanese, J.-C. Charlier, and X. Blase, Phys. Rev. Lett. **94**, 015503 (2005).
[24] S. Piscanec, M. Lazzeri, J. Robertson, A. C. Ferrari, and F. Mauri, Phys. Rev. B **75**, 035427 (2007).
[25] M. U. Kahaly and U. V. Waghmare, J. Nanosci. Nanotechnol. **7**, 1787 (2001).
[26] C. T. White, D. H. Robertson, and J. W. Mintmire, Phys. Rev. B **47**, 5485 (1993).
[27] V. N. Popov, V. E. Van Doren, and M. Balkanski, Phys. Rev. B **59**, 8355 (1999).
[28] V. N. Popov, V. E. Van Doren, and M. Balkanski, Phys. Rev. B **61**, 3078 (2000).
[29] J. Maultzsch, S. Reich, C. Thompsen, E. Dobardžić, I. Milošević, and M. Damnjanović, Solid State Commun. **121**, 471 (2002).
[30] V. N. Popov, Carbon **42**, 991 (2004).
[31] Y. N. Gartstein, Phys. Lett. A **327**, 83 (2004).
[32] J.-W. Jiang, H. Tang, B.-S. Wang, and Z.-B. Su, Phys. Rev. B **73**, 235434 (2006).
[33] N. V. Khokhryakov, S. S. Savinskiĭ, and J. M. Molina, JETP Lett. **62**, 617 (1995).
[34] E. Dobardžić, I. Milošević, B. Nikolić, T. Vuković, and M. Damnjanović, Phys. Rev. B **68**, 045408 (2003).
[35] I. Milošević, E. Dobardžić, and M. Damnjanović, Phys. Rev. B **72**, 085426 (2005).
[36] V. N. Popov and P. Lambin, Phys. Rev. B **73**, 085407 (2006).
[37] V. N. Popov and P. Lambin, Phys. Status Solidi B **243**, 34803484 (2006).
[38] V. N. Popov and P. Lambin, Physica E (Amsterdam) **37**, 97 (2007).
[39] J. W. Mintmire and C. T. White, Phys. Rev. Lett. **81**, 2506 (1998).

[40] C. T. White and J. W. Mintmire, J. Phys. Chem. B **109**, 52 (2005).
[41] P. B. Allen, Nano Lett. **7**, 11 (2007).
[42] J. W. Mintmire, B. I. Dunlap, and C. T. White, Phys. Rev. Lett. **68**, 631 (1992).
[43] N. Hamada, S. I. Sawada, and A. Oshiyama, Phys. Rev. Lett. **68**, 1579 (1992).
[44] R. Saito, M. Fujita, G. Dresselhaus, and M. S. Dresselhaus, Appl. Phys. Lett. **60**, 2204 (1992).
[45] E. B. Wilson, J. Chem. Phys. **7**, 1047 (1939).
[46] A. Grüneis, R. Saito, T. Kimura, L. G. Cançado, M. A. Pimenta, A. Jorio, A. G. Souza Filho, G. Dresselhaus, and M. S. Dresselhaus, Phys. Rev. B **65**, 155405 (2002).
[47] G. G. Samsonidze, R. Saito, A. Jorio, A. G. Souza Filho, A. Grüneis, M. A. Pimenta, G. Dresselhaus, and M. S. Dresselhaus, Phys. Rev. Lett. **90**, 027403 (2003).
[48] H. M. Lawler, D. Areshkin, J. W. Mintmire, and C. T. White, Phys. Rev. B **72**, 233403 (2005).